metals

MDPI

Article

Microwave Dielectric Behavior of $CoTiTa_2O_8$-$MgNb_2O_6$ Composite Ceramics: A Focus on Temperature Stability and Compositional Effects

Jun Zuo [1,2,3], Haodong Wang [2,*], Xiuli Fu [3] and Zhijian Peng [1,*]

[1] School of Science, China University of Geosciences, Beijing 100083, China; zuojun@email.cugb.edu.cn
[2] School of Engineering and Technology, China University of Geosciences, Beijing 100083, China
[3] School of Science, Beijing University of Posts and Telecommunications, Beijing 100876, China; xiulifu@bupt.edu.cn
* Correspondence: hdwang@cugb.edu.cn (H.W.); pengzhijian@cugb.edu.cn (Z.P.); Tel.: +86-10-8232-0255 (Z.P.)

Abstract: Microwave dielectric $(1-x)CoTiTa_2O_8$-$xMgNb_2O_6$ composite ceramics (x = 0.625–0.725) were fabricated through a two-step method and sintering techniques. The applied $CoTiTa_2O_8$ and $MgNb_2O_6$ powders were both synthesized by calcining stoichiometric mixtures of their respective metal oxides at 1000 °C for 3 h. The optimal sintering parameters were determined using visual high-temperature deformation analysis. The influence of the $MgNb_2O_6$ content on the phase composition, microstructure, and microwave dielectric properties of the obtained composite ceramics was comprehensively investigated. It was observed that an increase in the $MgNb_2O_6$ content resulted in a reduction in the dielectric constant (ε_r) and a significant enhancement in the quality factor ($Q \times f$). The ceramics with a compositional value of x = 0.675, sintered at 1193 °C for 4.5 h, demonstrated a near-zero temperature coefficient of the resonant frequency (τ_f), exhibiting optimal microwave dielectric properties: ε_r = 28.4, $Q \times f$ = 33,055 GHz, and τ_f = −3.1 ppm/°C. These findings underscore the potential of the present $CoTiTa_2O_8$-$MgNb_2O_6$ composite ceramics for advanced microwave applications.

Keywords: composite ceramics; $CoTiTa_2O_8$; $MgNb_2O_6$; sintering; microwave dielectric properties

check for updates

Academic Editor: Slobodan Mitrovic

Received: 2 March 2025
Revised: 27 March 2025
Accepted: 31 March 2025
Published: 4 April 2025

Citation: Zuo, J.; Wang, H.; Fu, X.; Peng, Z. Microwave Dielectric Behavior of $CoTiTa_2O_8$-$MgNb_2O_6$ Composite Ceramics: A Focus on Temperature Stability and Compositional Effects. *Metals* **2025**, *15*, 407. https://doi.org/10.3390/met15040407

Copyright: © 2025 by the authors. Licensee MDPI, Basel, Switzerland. This article is an open access article distributed under the terms and conditions of the Creative Commons Attribution (CC BY) license (https://creativecommons.org/licenses/by/4.0/).

1. Introduction

The rapid advancement of 5G communication technology has ushered in a new era of telecommunications, triggering an unprecedented demand for high-performance microwave components, driving the development of advanced materials with superior functionality and reliability [1]. Among these, microwave dielectric ceramics have emerged as indispensable materials in modern communication systems, playing a pivotal role in the fabrication of resonators, filters, dielectric substrates, antennas, waveguide circuits, and so on [2–5]. These components are fundamental to the functionality of modern wireless communication systems, enabling enhanced data transmission rates, broader bandwidth, and superior signal integrity. However, the relentless evolution of 5G and the imminent arrival of 6G technologies necessitate the development of microwave dielectric ceramics with exceptional properties to meet the increasingly stringent performance requirements of next-generation communication systems [6–8].

To meet the stringent requirements of next-generation communication technologies [9,10], high-performance microwave dielectric ceramics must simultaneously satisfy

three critical criteria: (i) an appropriate relative dielectric constant (ε_r) to facilitate the miniaturization of devices, (ii) a high quality factor ($Q \times f$) or low dielectric loss to ensure energy efficiency [11], and (iii) a near-zero temperature coefficient of the resonant frequency [12] (τ_f) to guarantee stability under varying operating conditions [13]. Nevertheless, single-phase ceramic materials often exhibit inherent limitations, making it challenging to simultaneously achieve all these desired properties. Consequently, researchers have turned to composite materials as a viable strategy to optimize the overall performance of microwave dielectric ceramics.

In recent years, the $ATiB_2O_8$ ceramic series (where A = Mg^{2+}, Zn^{2+}, Cu^{2+}, Co^{2+}, Ni^{2+}; B = Ta^{5+}, Nb^{5+}) have garnered considerable attention due to their remarkable microwave dielectric properties [14]. For instance, Yang et al. [15] synthesized $CoTiTa_2O_8$ ceramics via a conventional solid-phase reaction method, achieving a dielectric constant (ε_r) of 40.69 and a quality factor ($Q \times f$) of 17,291 GHz when the ceramics were sintered at 1075 °C. Despite these promising attributes, the material exhibited a large positive temperature coefficient of the resonant frequency (τ_f = +114.54 ppm/°C), resulting in inadequate thermal stability and hindering its practical applicability. To address this issue, researchers have explored the strategy of combining materials with opposite τ_f values to achieve near-zero temperature coefficients [16–19]. This approach has proven effective in various material systems. For instance, Wu et al. [20] demonstrated that in $(1 - x)CoTiNb_2O_8$-$xZnNb_2O_6$ composites, a τ_f value of +3.57 ppm/°C could be achieved at x = 0.5, alongside a dielectric constant (ε_r) of 39.2 and a quality factor ($Q \times f$) of 40,013 GHz. Similarly, Jiang et al. [21] demonstrated that in $(1 - x)MgZrTa_2O_8$-$xMgTa_2O_6$ composites, a near-zero τ_f value of −0.57 ppm/°C was obtained at x = 0.75, with ε_r = 24.88 and $Q \times f$ = 26,823 GHz. These studies underscore the efficacy of composite strategies in tailoring microwave dielectric properties to meet specific application requirements.

Despite these advancements, the development of composite ceramics incorporating $CoTiTa_2O_8$ remains largely unexplored, presenting a significant research gap. This gap presents a significant opportunity, particularly considering $CoTiTa_2O_8$'s characteristics of having a low sintering temperature (1366 °C) [15] while exhibiting a large positive temperature coefficient of the resonant frequency (τ_f), along with its compatibility with other niobate-tantalate systems for high-performance applications [22–25]. Notably, $MgNb_2O_6$ (with a sintering temperature of 1309 °C) ceramics, which exhibit a large negative τ_f value (−70 ppm/°C) and belong to the same niobate-tantalate family as $CoTiTa_2O_8$, offer an ideal counterpart to $CoTiTa_2O_8$ due to their complementary temperature stability characteristics. For instance, Tzou et al. [26] reported that $MgNb_2O_6$ ceramics possess a dielectric constant (ε_r) of 21.4, a quality factor ($Q \times f$) of 93,800 GHz, and a τ_f value of −70 ppm/°C [27]. These properties suggest that combining $CoTiTa_2O_8$ with $MgNb_2O_6$ could yield a composite material with a near-zero τ_f, thereby addressing the thermal stability issue while maintaining desirable dielectric properties. Furthermore, recent studies by Yang et al. [28] and Shi et al. [29] have highlighted the potential of niobate-tantalate-based [30–33] composites in achieving superior microwave dielectric performance, further supporting the rationale for such investigations.

In light of the above review, this study aimed to develop $(1 - x)CoTiTa_2O_8$-$xMgNb_2O_6$ (x = 0.625–0.725) composite ceramics with enhanced temperature stability and low dielectric loss. The influence of the $MgNb_2O_6$ content on the phase composition, microstructure, and microwave dielectric properties of the obtained composite ceramics was comprehensively investigated. This work not only advances the understanding of $CoTiTa_2O_8$-based composite ceramics but also provides a pathway for designing high-performance microwave dielectric ceramics tailored for 5G and future communication technologies.

2. Experimental Section

2.1. Sample Preparation

High-purity powders of CoO (99.7%), TiO_2 (99.0%), Ta_2O_5 (99.5%), MgO (99.7%), and Nb_2O_5 (99.9%) were selected as raw materials. The powders were weighed according to the stoichiometric ratios of $CoTiTa_2O_8$ and $MgNb_2O_6$ and then mixed in a corundum jar with zirconia balls as the grinding media and absolute ethanol as dispersive media, respectively. The mixtures were ball-milled for 6 h in a planetary ball mill to ensure homogeneity [34]. After ball-milling, the resulting slurries were dried at 80 °C for 12 h. The dried powders were then calcined at 1000 °C for 3 h in a muffle furnace using a conventional solid-phase reaction method to synthesize $CoTiTa_2O_8$ and $MgNb_2O_6$ powders, respectively [35–37]. Afterwards, the calcined $CoTiTa_2O_8$ and $MgNb_2O_6$ powders were weighed in specific proportions to prepare $(1 - x)CoTiTa_2O_8$-$xMgNb_2O_6$ (x = 0.625–0.725) composite powders. These composite powders were subjected to a second round of ball-milling under the same conditions (in planetary mill for 6 h with zirconia balls and absolute ethanol) to ensure uniform mixing. The resulting slurries were dried again, and the dried powders were uniaxially pressed into cylindrical green bodies at a pressure of 8 MPa for 60 s. The green bodies had a diameter of 12 mm and a height of 5–6 mm. Finally, the samples were sintered in a muffle furnace at 1193 °C for 4.5 h in an air atmosphere. Notably, the optimal sintering conditions for the samples were determined using a visual high-temperature deformation analyzer (TA-16A01, Tianjin Zhonghuan Experimental Furnace Co., Ltd., Tianjin, China).

2.2. Materials Characterization

The apparent density of the sintered samples was measured by the Archimedes method in accordance with ISO 18754. The relative density was calculated as the ratio of the apparent density to the theoretical density, expressed as a percentage. The crystalline phases of the sintered samples were characterized by X-ray diffraction (XRD, D/max-RB, Rigaku, Tokyo, Japan) with Cu Kα radiation (λ = 1.5406 Å). The XRD patterns were recorded in the 2θ range of from 10° to 85° at a scanning rate of 4° per minute. The microstructural features of the samples were examined using field emission scanning electron microscopy (FE-SEM, ZEISS Gemini SEM 500, ZEISS, Oberkochen, Germany), and the average grain size was calculated from the SEM images using the Nano Measurer 1.2 software.

As shown in Figure 1, the dual-channel signal cables of the Keysight E5063A network analyzer (USA) were connected to the resonant cavity. A sintered ceramic disc (12 mm diameter × 5–6 mm thickness) was positioned at the cavity center, and the assembly was secured by tightening the screws. In the TE01δ mode, the microwave dielectric constant (ε_r) and quality factor ($Q \times f$) were measured using the cavity perturbation method, with the input parameters of the ceramic disc's diameter and thickness obtained after sintering at 25 °C and 85 °C, respectively. While ε_r, Q, and the resonant frequency f were directly recorded, the temperature coefficient of the resonant frequency τ_f was determined by Equation (1):

$$\tau_f = \frac{f_{T2} - f_{T1}}{f_{T1}(T_2 - T_1)} \times 10^6 (\text{ppm}/^\circ\text{C}) \quad (1)$$

where f_{T1} and f_{T2} represent the resonant frequencies of the specimens at T_1 (25 °C) and T_2 (85 °C), respectively.

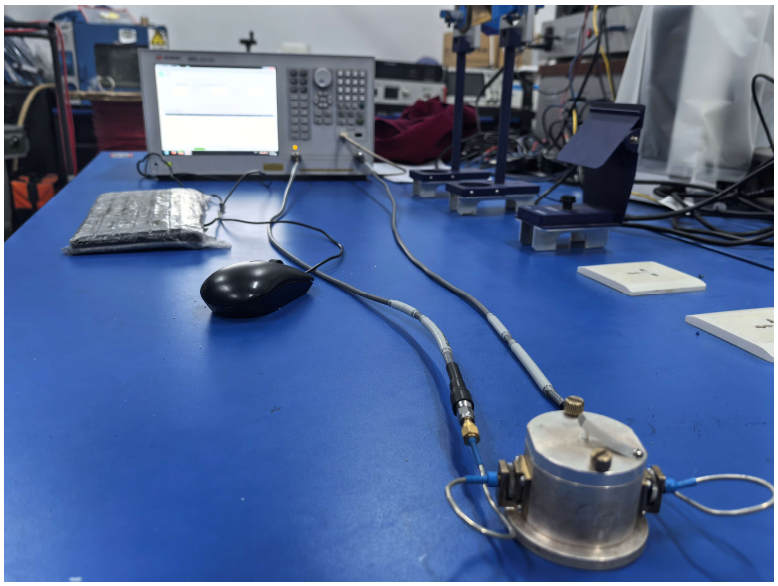


Figure 1. Photograph of the experimental setup.

3. Results and Discussion

3.1. Sintering Behavior

The sintering behavior of the designed (1 − x)$CoTiTa_2O_8$-x$MgNb_2O_6$ (x = 0.625–0.725) composite ceramics was systematically investigated using a visual high-temperature deformation analyzer. Figure 2a–e illustrates the shrinkage amount and shrinkage rate with temperature for the samples of different compositions. For the samples with x = 0.625, 0.65, 0.675, 0.7, and 0.725, the maximum shrinkage rates were observed at approximately 1193, 1178, 1169, 1165, and 1163 °C, respectively. The completion of shrinkage occurred at 1362, 1342, 1327, 1317, and 1312 °C for the respective compositions of the samples. To ensure uniform densification across all samples [38], the highest temperature among the maximum shrinkage rates (1193 °C) was selected as the optimal sintering temperature [39] for all the samples. Furthermore, the holding time was determined by analyzing the shrinkage behavior of a typical sample with a nominal composition of 0.275$CoTiTa_2O_8$-0.725$MgNb_2O_6$ at 1193 °C (see Figure 2f). The results revealed that, in this case, the shrinkage rate dropped to zero after approximately 4.5 h, indicating that it was completely densified. Thus, the optimal sintering conditions were determined to be 1193 °C for 4.5 h.

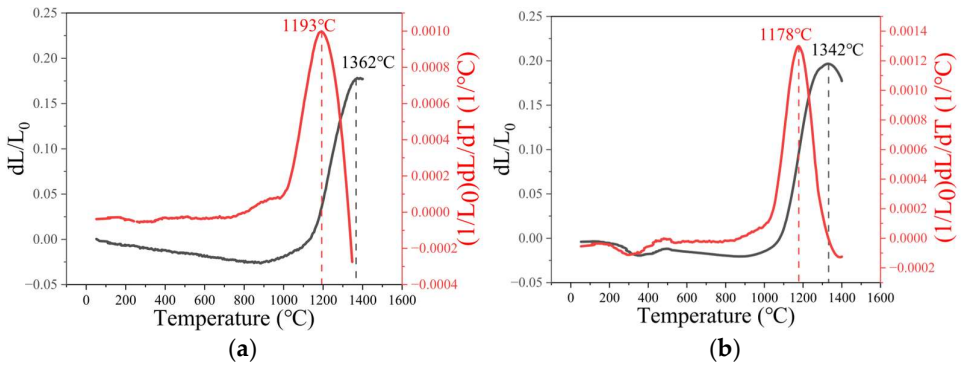


Figure 2. *Cont.*

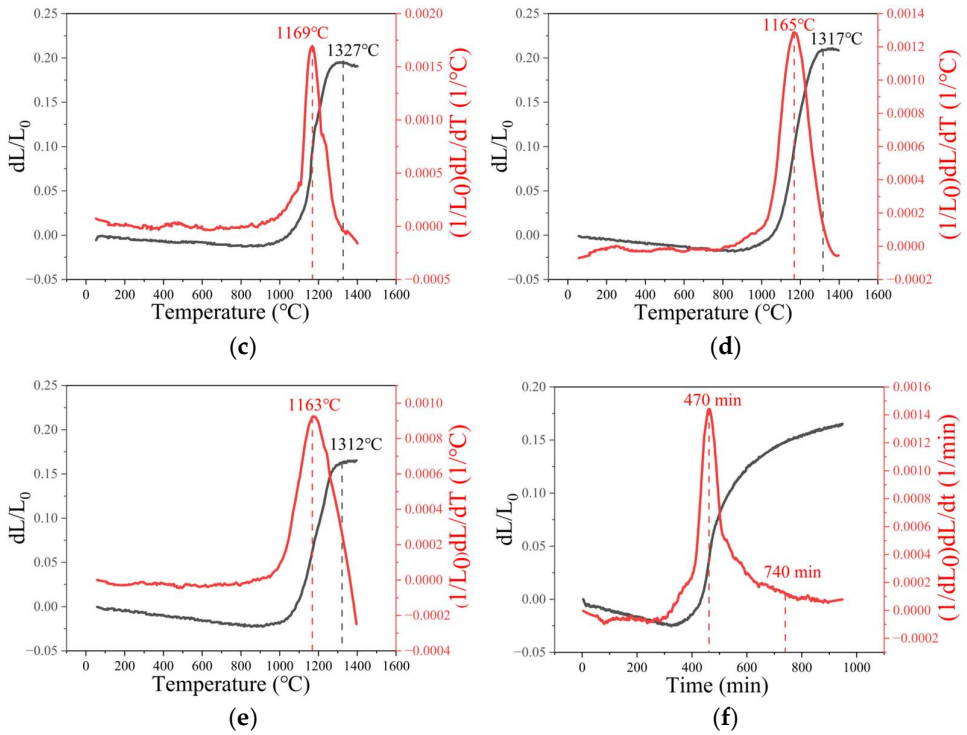


Figure 2. Shrinkage behavior of the designed (1 − x)$CoTiTa_2O_8$-x$MgNb_2O_6$ composite ceramics with temperature: (**a**) x = 0.625, (**b**) x = 0.65, (**c**) x = 0.675, (**d**) x = 0.7, and (**e**) x = 0.725. Shrinkage behavior of a typical sample with a nominal composition of 0.275$CoTiTa_2O_8$-0.725$MgNb_2O_6$ as a function of time when sintered at 1193 °C for 4.5 h (**f**).

3.2. Phase Composition and Microstructure

X-ray diffraction (XRD) analysis was performed to identify the crystalline phases in the sintered ceramics. As shown in Figure 3, the XRD patterns of the resultant (1 − x)$CoTiTa_2O_8$-x$MgNb_2O_6$ (x = 0.625–0.725) composite ceramics exhibited characteristic peaks corresponding to $CoTiTa_2O_8$ and $MgNb_2O_6$. For instance, the (110) peak of $CoTiTa_2O_8$ was observed at 26.6°, while the (311) peak of $MgNb_2O_6$ appeared at 30.2°. All minor peaks in the collected patterns could be indexed to the standard cards of $CoTiTa_2O_8$ (at present, ICDD does not have a standard card for $CoTiTa_2O_8$, so we used the similar $CoTa_2O_6$ JCPDS #84-2063 instead.) and $MgNb_2O_6$ (JCPDS #88-0708), confirming the absence of secondary phases. This result indicates that the obtained ceramics consisted solely of $CoTiTa_2O_8$ and $MgNb_2O_6$ phases, with no detectable impurities or intermediate phases.

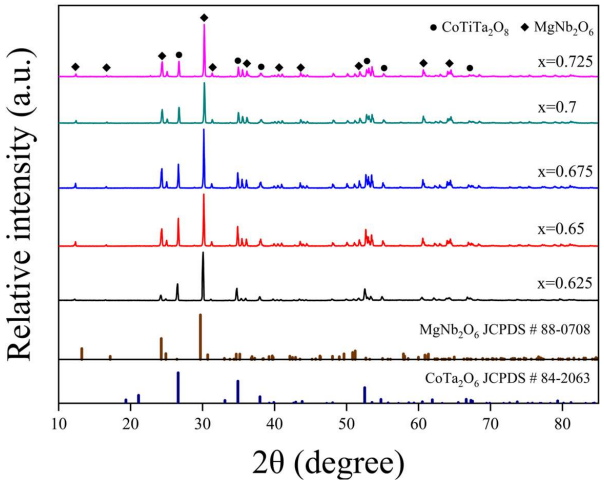


Figure 3. XRD patterns of (1 − x)$CoTiTa_2O_8$-x$MgNb_2O_6$ ceramics sintered at 1193 °C for 4.5 h.

The microstructures of the obtained (1 − x)$CoTiTa_2O_8$-x$MgNb_2O_6$ composite ceramics were examined using scanning electron microscopy (SEM). Figure 4a–e display the fresh fractural surface morphology of the obtained ceramics. As is seen in these images, the $CoTiTa_2O_8$ crystals exhibited a distinct disc-like morphology [26], while the $MgNb_2O_6$ crystals appeared as smaller round rods. Statistical analysis of the grain size distribution (see Figure 4f) revealed that the average grain size of the $CoTiTa_2O_8$ and $MgNb_2O_6$ increased with the addition amount of $MgNb_2O_6$. This trend suggests that the addition of $MgNb_2O_6$ promotes the grain growth of $CoTiTa_2O_8$ during sintering.

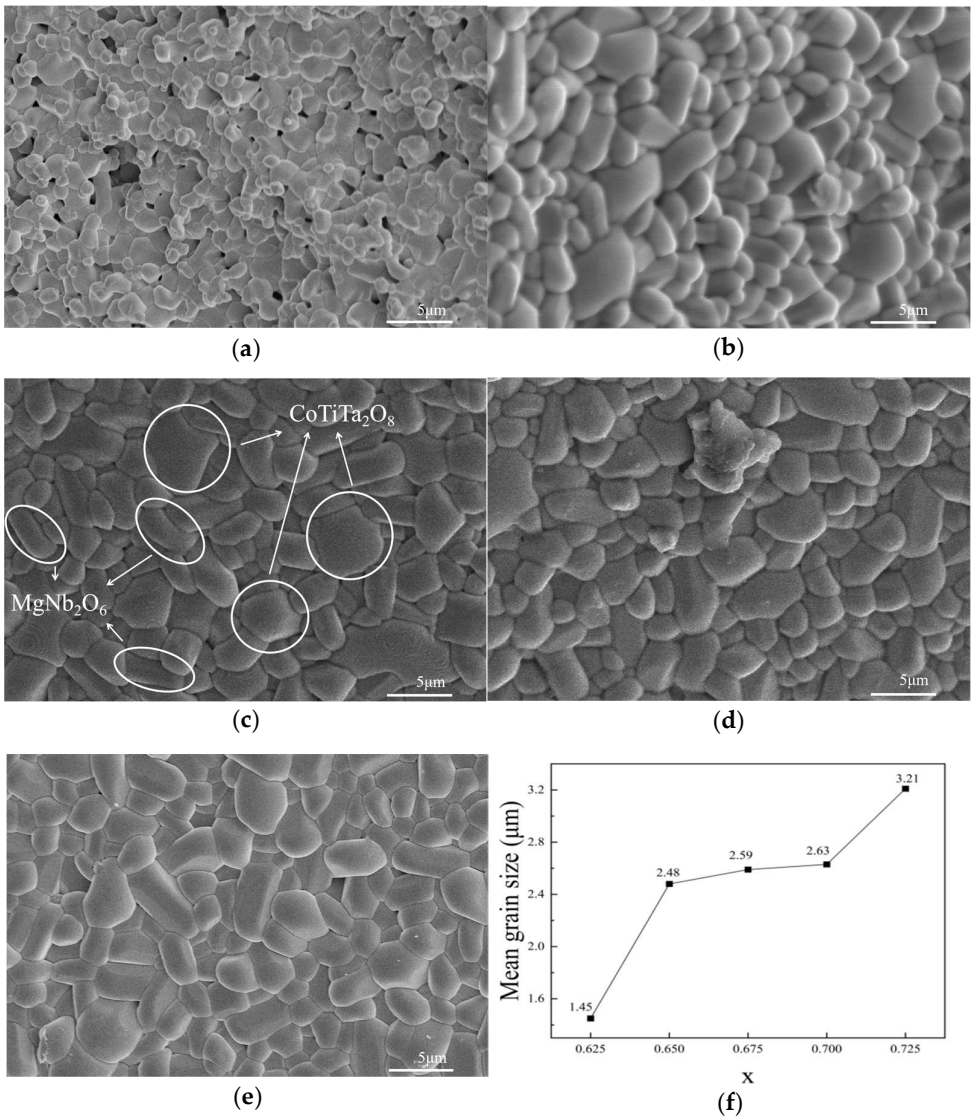


Figure 4. SEM images on the fresh fractural surface of the obtained (1 − x)$CoTiTa_2O_8$-x$MgNb_2O_6$ (x = 0.625–0.725) composite ceramics sintered at 1193 °C for 4.5 h: (**a**) x = 0.625, (**b**) x = 0.65, (**c**) x = 0.675, (**d**) x = 0.7, and (**e**) x = 0.725, and grain size distribution with x (**f**).

To further investigate the elemental composition and distribution in the obtained ceramics, SEM–mapping imaging and EDS analysis were performed on a typical sample with x = 0.675 (Figure 5). The results demonstrated a homogeneous distribution of Mg, Nb, O, Co, Ta, and Ti elements within the crystals in the ceramics. Notably, Mg, Nb, and O were predominantly concentrated around the $CoTiTa_2O_8$ crystals, indicating the formation of a solid solution between the $CoTiTa_2O_8$ and $MgNb_2O_6$. Under prolonged high–low temperature cycling, cation interdiffusion (e.g., $Co^{2+} \leftrightarrow Mg^{2+}$) at interfaces may have formed a non-stoichiometric transition layer. Excessive diffusion rates could lead to the formation

of low-permittivity or high-loss secondary phases (e.g., spinel-like structures), degrading high-frequency performance. Additionally, the diffusion-induced compositional gradient at interfaces may alter the local oxygen vacancy concentration, thereby influencing dielectric relaxation behavior (observable through temperature-dependent permittivity spectra).

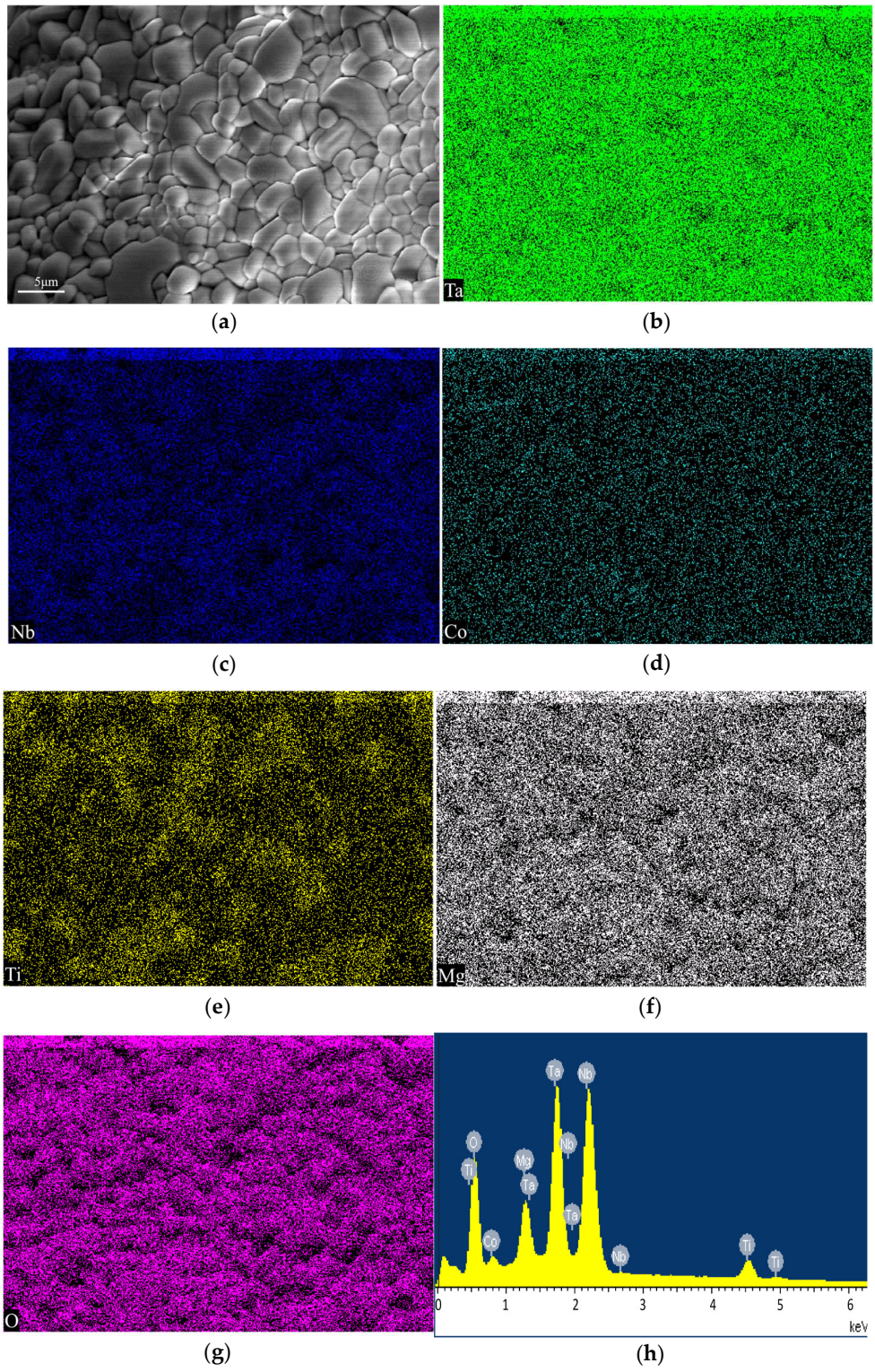


Figure 5. (**a**) SEM image of a typical sample with a nominal composition of$0.325CoTiTa_2O_8$-$0.675MgNb_2O_6$. Elemental mapping image of $0.325CoTiTa_2O_8$-$0.675MgNb_2O_6$ ceramics: (**b**) Ta, (**c**) Nb, (**d**) Co, (**e**) Ti, (**f**) Mg, and (**g**) O, and EDS analysis result (**h**).

Fracture surface analysis provided additional insights into the densification behavior. Figure 6 shows the SEM images of the fresh fracture surfaces of the obtained $(1-x)CoTiTa_2O_8$-$xMgNb_2O_6$ (x = 0.625–0.725) composite ceramics under a magnification of 500 times. As is seen, when the $MgNb_2O_6$ content increased, the porosity of the ceramics decreased significantly. This can be attributed to the lower sintering temperature of $MgNb_2O_6$ (~1309 °C) [40] compared to $CoTiTa_2O_8$ (~1366 °C) [15], which facilitated the elimination of pores during sintering and promoted grain growth.

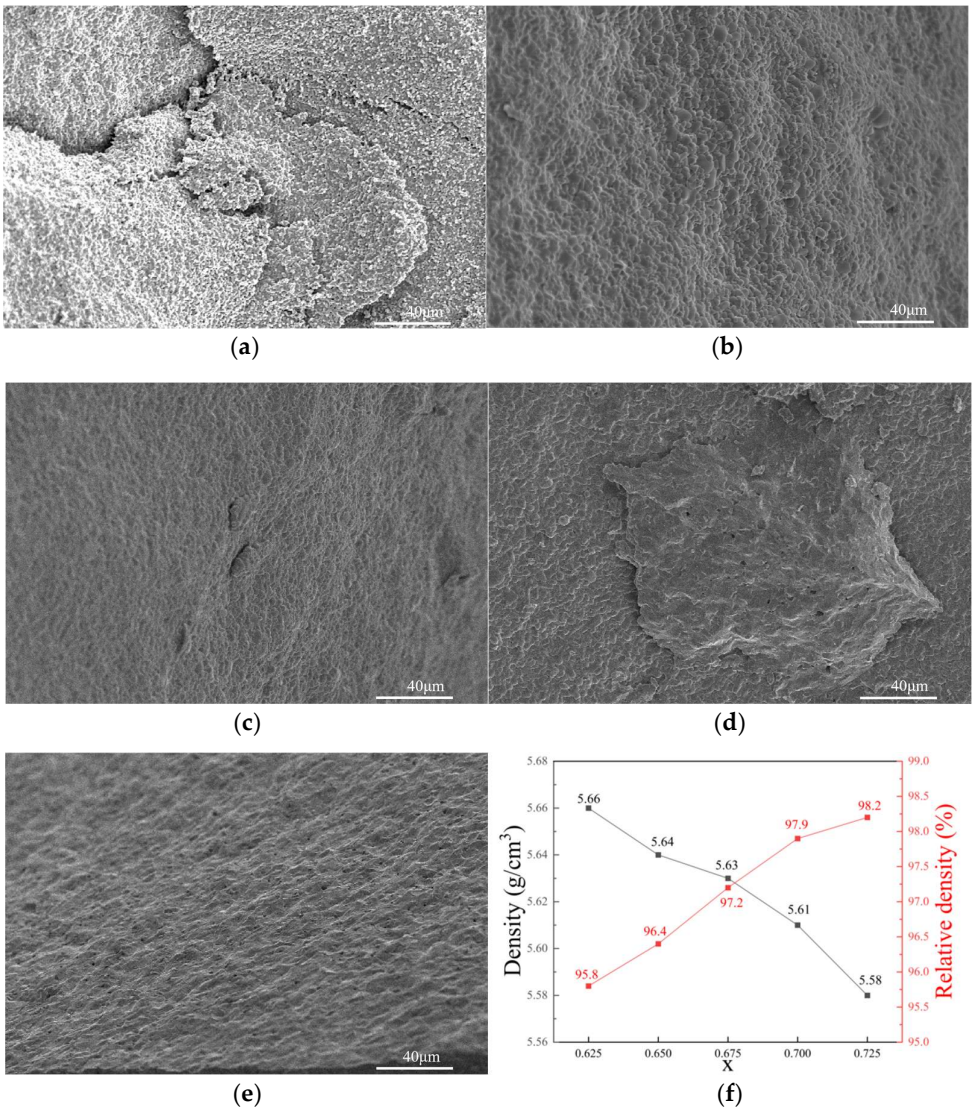


Figure 6. SEM images on the fresh fractural surface of the obtained $(1-x)CoTiTa_2O_8$-$xMgNb_2O_6$ composite ceramics sintered at 1193 °C for 4.5 h under a magnification of 500 times: (**a**) x = 0.625, (**b**) x = 0.65, (**c**) x = 0.675, (**d**) x = 0.7, and (**e**) x = 0.725, and density and relative density with x (**f**).

The density and relative density of the $(1-x)CoTiTa_2O_8$-$xMgNb_2O_6$ composite ceramics are presented in Figure 6f. While the absolute density decreased with increasing the $MgNb_2O_6$ content due to its lower density compared to that of $CoTiTa_2O_8$, the relative density exhibited an upward trend. This indicates that the addition of $MgNb_2O_6$ enhanced the densification of the ceramics, consistent with the reduced porosity observed in the SEM images (see Figure 6a–e).

3.3. Microwave Dielectric Properties

The dielectric constant (ε_r) of the obtained ceramics decreased with a higher $MgNb_2O_6$ content, as shown in Figure 7a. This behavior was attributed to the lower dielectric constant of $MgNb_2O_6$ relative to that of $CoTiTa_2O_8$.

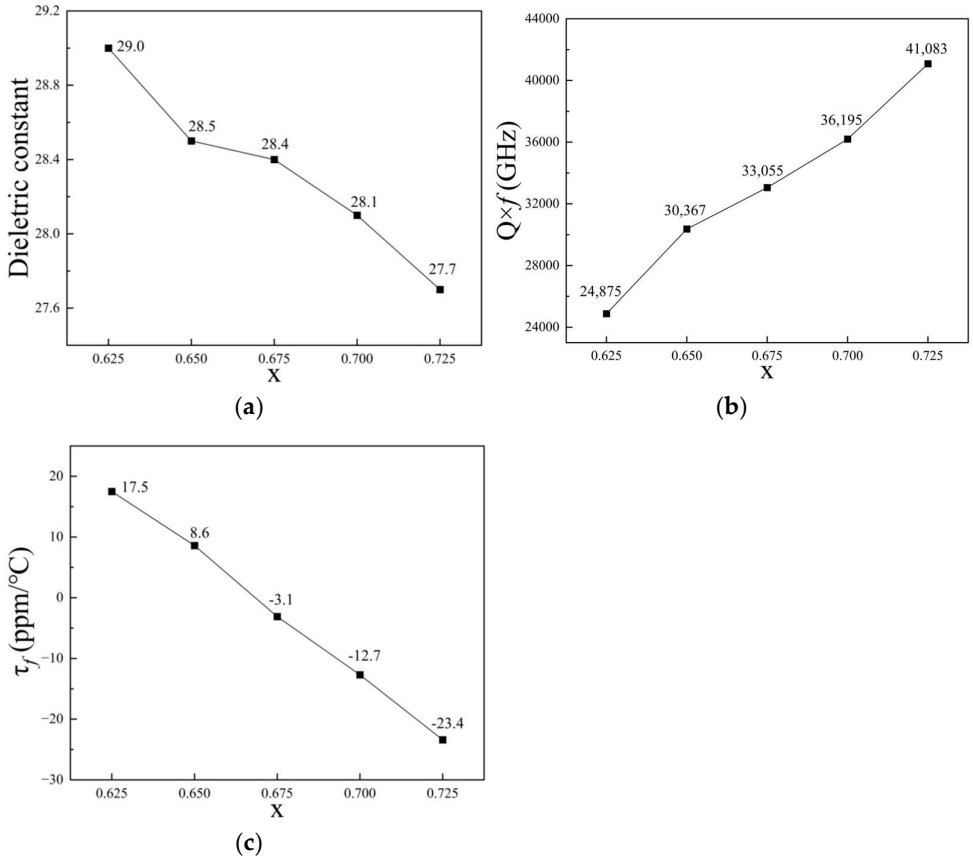


Figure 7. Variations in (**a**) the dielectric constant, (**b**) quality factor, and (**c**) temperature coefficient of the resonant frequency with the $MgNb_2O_6$ content for the resultant $(1-x)CoTiTa_2O_8$-$xMgNb_2O_6$ (x = 0.625–0.725) composite ceramics sintered at 1193 °C for 4.5 h.

The quality factor ($Q \times f$) exhibited a significant improvement with increasing x (Figure 7b). This enhancement can be explained by two factors: (1) the intrinsic high $Q \times f$ value of $MgNb_2O_6$ (93,800 GHz) compared to that of $CoTiTa_2O_8$ (17,291 GHz), and (2) the reduction in grain boundary defects as the grain size increased, which minimized dielectric losses.

The temperature coefficient of the resonant frequency (τ_f) of the obtained ceramics decreased with a higher $MgNb_2O_6$ content, as illustrated in Figure 7c. This trend was due to the negative τ_f value of $MgNb_2O_6$, which compensated for the positive τ_f of $CoTiTa_2O_8$. Notably, the composition with x = 0.675 exhibited a τ_f value closest to zero (−3.1 ppm/°C), making it a promising candidate for applications requiring stable microwave dielectric properties.

4. Conclusions

In this study, the sintering behavior, microstructure, and microwave dielectric properties of $(1-x)CoTiTa_2O_8$-$xMgNb_2O_6$ (x = 0.625–0.725) composite ceramics were investigated. The optimal sintering conditions were determined to be 1193 °C for 4.5 h by using a visual high-temperature deformation analyzer, ensuring dense sintering for all compositions. In the resultant ceramics, only $CoTiTa_2O_8$ and $MgNb_2O_6$ phases were detected, implying no additional phases. Increasing the $MgNb_2O_6$ content (x) led to larger grain sizes and

higher relative densities, which could be attributed to the lower sintering temperature of $MgNb_2O_6$.

The dielectric constant (ε_r) and temperature coefficient of the resonant frequency (τ_f) decreased with higher x, while the quality factor ($Q \times f$) significantly was improved due to the intrinsic properties of $MgNb_2O_6$ and reduced grain boundary defects. The composition with x = 0.675 exhibited optimal performance, with $\tau_f = -3.1$ ppm/°C, $\varepsilon_r = 28.4$, and $Q \times f = 33{,}055$ GHz.

These results demonstrate that adjusting the $MgNb_2O_6$ content effectively optimizes the microstructure and microwave dielectric properties of $CoTiTa_2O_8$-$MgNb_2O_6$ composite ceramics, making them suitable for high-performance dielectric applications. The high $Q \times f$ value (33,055 GHz) indicates that the material exhibits low-loss characteristics in high-frequency bands (millimeter-wave bands), making it suitable for dielectric filters and resonators in 5G/6G base stations, which can enhance signal transmission efficiency and reduce energy consumption. The combination of a moderate dielectric constant ($\varepsilon_r = 28.4$) and low loss suggests its applicability as a millimeter-wave antenna array substrate, supporting high-density integration and miniaturized designs. The temperature stability (τ_f close to zero) allows for adaptation to extreme temperature variations in space environments, ensuring controllable frequency drift, which demonstrates its potential for use in low-Earth-orbit (LEO) satellite phased-array antennas and on-board filters. These are some potential applications of $CoTiTa_2O_8$-$MgNb_2O_6$ composite ceramics.

The experimental results of this paper show that there are still many problems in the study of $CoTiTa_2O_8$-$MgNb_2O_6$ composite microwave dielectric ceramics that need to be further explored: (1) The preparation process has certain effects on the sintering temperature and dielectric properties of microwave dielectric ceramics. Therefore, new preparation processes such as the molten salt method and co-precipitation method can be explored to prepare ceramic powders, and sintering technologies such as discharge plasma sintering and microwave sintering can be used to prepare ceramics so as to obtain a better performance of $CoTiTa_2O_8$-$MgNb_2O_6$ composite microwave dielectric ceramics. (2) The use of sintering additives can reduce the sintering temperature of ceramics to a certain extent. However, the sintering temperature of $CoTiTa_2O_8$-$MgNb_2O_6$ composite microwave dielectric ceramics is still too high to be used in low-temperature co-firing technology. Therefore, suitable sintering additives can be found, which can not only reduce the sintering temperature of ceramics but can also better maintain the dielectric properties of ceramics. (3) In this paper, $CoTiTa_2O_8$-$MgNb_2O_6$ composite microwave dielectric ceramics with good performance were obtained from an experimental point of view, and device design and simulation can be further carried out to explore the feasibility of their practical application.

Author Contributions: Conceptualization, J.Z.; investigation, J.Z.; validation, J.Z. and H.W.; formal analysis, H.W.; resources, X.F.; data curation, H.W.; writing—original draft preparation, J.Z. and H.W.; writing—review and editing, X.F. and Z.P.; supervision, X.F. and Z.P.; project administration, Z.P. All authors have read and agreed to the published version of the manuscript.

Funding: This work was supported by the open research fund of Songshan Lake Materials Laboratory (2023SLABFK10) and National Natural Science Foundation of China (grant nos. 12174035 and 61274015).

Data Availability Statement: The original contributions presented in the study are included in the article; further inquiries can be directed to the corresponding author.

Conflicts of Interest: The authors declare that they have no known competing financial interests or personal relationships that could have appeared to influence the work reported in this paper.

References

1. Miao, Y.; Yang, K.; Zhao, P.; Yang, Z.H.; Yu, X.Y.; Duan, X.M.; Jia, D.C.; Zhou, Y. Development of industry system of microwave dielectric ceramics. *Strateg. Study Chin. Acad. Eng.* **2024**, *26*, 34–41.
2. Raveendran, A.; Sebastian, M.T.; Raman, S. Applications of microwave materials: A review. *J. Electron. Mater.* **2019**, *48*, 2601–2634.
3. Pang, Q.Y.; Chen, Y.; Wang, Z.X.; Zhou, B.; Li, X.; Mu, C.; Gu, G.P.; Wang, G.S. Structure, electric, and dielectric properties of $(Sr_{0.7}Ca_{0.3})_{1.02}(Zr_{0.95-x}Ti_{0.05}Mn_x)O_{3+\delta}$ ceramics for BME-MLCCs application. *J. Adv. Ceram.* **2024**, *13*, 1382–1393.
4. Feng, C.; Zhou, X.; Tao, B.J.; Wu, H.T.; Huang, S.F. Crystal structure and enhanced microwave dielectric properties of the $Ce_2[Zr_{1-x}(Al_{1/2}Ta_{1/2})_x]_3(MoO_4)_9$ ceramics at microwave frequency. *J. Adv. Ceram.* **2022**, *11*, 392–402. [CrossRef]
5. Guo, W.J.; Ma, Z.Y.; Luo, Y.; Chen, Y.G.; Yue, Z.X.; Li, L.T. Structure, defects, and microwave dielectric properties of Al-doped and Al/Nd co-doped $Ba_4Nd_{9.33}Ti_{18}O_{54}$ ceramics. *J. Adv. Ceram.* **2022**, *11*, 629–640. [CrossRef]
6. Tan, K.; Song, T.; Shen, T.; Yu, H.L.; Zhang, Y.C.; Cui, K.; Xu, X.B.; Li, W.; Wang, H.R. Research progress of low permittivity microwave dielectric ceramics. *Adv. Ceram.* **2022**, *43*, 11–29.
7. Bao, J.; Zhang, Y.P.; Kimura, H.D.; Wu, H.T.; Yue, Z.X. Crystal structure, chemical bond characteristics, infrared reflection spectrum, and microwave dielectric properties of $Nd_2(Zr_{1-x}Ti_x)_3(MoO_4)_9$ ceramics. *J. Adv. Ceram.* **2023**, *12*, 82–92.
8. Tian, H.; Zhang, X.H.; Zhang, Z.D.; Liu, Y.; Wu, H. Low-permittivity $LiLn(PO_3)_4$ (Ln = La, Sm, Eu) dielectric ceramics for microwave/millimeter-wave communication. *J. Adv. Ceram.* **2024**, *13*, 602–620. [CrossRef]
9. Du, Q.B.; Jiang, L.X.; Ma, L.Z.; Duan, J.H.; Zhou, Z.Y.; Li, H. Lattice evolution, order transformation, and microwave dielectric properties of the $Zn_{1-x}Li_{2x}TiO_3$ ($0 \leq x \leq 1$) system ceramics. *J. Adv. Ceram.* **2024**, *13*, 1178–1188.
10. Li, J.M.; Wang, Z.X.; Guo, Y.F.; Ran, S.L. Influences of substituting of $(Ni_{1/3}Nb_{2/3})^{4+}$ for Ti^{4+} on the phase compositions, microstructures, and dielectric properties of $Li_2Zn[Ti_{1-x}(Ni_{1/3}Nb_{2/3})_x]_3O_8$ ($0 \leq x \leq 0.3$) microwave ceramics. *J. Adv. Ceram.* **2023**, *12*, 760–777.
11. Zhang, Y.H.; Xiang, H.C.; Wu, X.Y.; Zhou, Y.; Tang, Y.; Fang, L. Low dielectric loss in vanadium-based zircon ceramics via high-entropy strategy. *J. Adv. Ceram.* **2025**, *14*, 9221012.
12. Yang, Y.; Fang, W.S.; Lin, H.X.; Li, J.; Xiang, H.C.; Tang, Y.; Li, L.; Fang, L. $SrGa_{12}O_{19}$: The first low-ε_r Ga-based microwave dielectric ceramic with anomalous positive τ_f. *J. Adv. Ceram.* **2024**, *13*, 1432–1441.
13. Zhang, P.; Lin, J.; Jia, Q.; Yang, X.J.; Li, H. Research progress and prospect of microwave dielectric ceramic materials for 5G communication. *Adv. Ceram.* **2024**, *45*, 44–58.
14. Pan, H.L.; Cheng, L.; Mao, Y.X. Investigation and characterization on crystal structure of ixiolite structure $ATiNb_2O_8$ (A = Mg, Zn) ceramics at microwave frequency based on the complex chemical bond theory. *J. Alloys Compd.* **2017**, *693*, 792–798.
15. Yang, H.Y.; Zhang, S.R.; Chen, Y.W.; Yang, H.C.; Yuan, Y.; Li, E.Z. Crystal chemistry, raman spectra, and bond characteristics of trirutile-type $Co_{0.5}Ti_{0.5}TaO_4$ microwave dielectric ceramics. *Inorg. Chem.* **2019**, *58*, 968–976.
16. Kumada, N.; Koike, N.; Nakanome, K.; Yanagida, S.; Takei, T.; Miura, A.; Magome, E.; Moriyoshi, C.; Kuroiwa, Y. Synthesis of rutile-type solid solution $Ni_{1-x}Co_xTi(Nb_{1-y}Ta_y)_2O_8$ ($0 \leq x \leq 1$, $0 \leq y \leq 1$) and its optical property. *J. Asian Ceram. Soc.* **2017**, *5*, 284–289.
17. Liao, Q.W.; Li, L.X.; Zhang, P.; Cao, L.F.; Han, Y.M. Correlation of crystal structure and microwave dielectric properties for $ZnTi(Nb_{1-x}Ta_x)_2O_8$ ceramics. *Solid State Sci.* **2011**, *13*, 1201–1204.
18. Park, J.H.; Choi, Y.J.; Nahm, S.; Park, J.G. Crystal structure and microwave dielectric properties of $ZnTi(Nb_{1-x}Ta_x)_2O_8$ ceramics. *J. Alloys Compd.* **2011**, *509*, 6908–6912.
19. Zhang, Y.; Ding, S.H.; You, L.; Zhang, Y.C. Temperature stable microwave dielectric ceramic $CoTiNb_2O_8$-$Zn_{1.01}Nb_2O_6$ with ultra-low dielectric loss. *J. Electron. Mater.* **2019**, *48*, 867–872.
20. Wu, M.J.; Zhang, Y.C.; Xiang, M.Q. Synthesis, characterization and dielectric properties of a novel temperature stable (1-x)$CoTiNb_2O_8$-x$ZnNb_2O_6$ ceramic. *J. Adv. Ceram.* **2019**, *8*, 228–237.
21. Jiang, X.; Guo, X.R.; Zhang, Y.; Ding, S.H.; Song, T.X. A novel (1-x)$MgZrTa_2O_8$-x$MgTa_2O_6$ microwave dielectric composite ceramic with near-zero temperature coefficient. *J. Mater. Sci. Mater. Electron.* **2023**, *34*, 660.
22. Yang, H.Y.; Chai, L.; Liang, G.C.; Xing, M.J.; Fang, Z.X.; Zhang, X.; Qin, T.Y.; Li, E.Z. Structure, far-infrared spectroscopy, microwave dielectric properties, and improved low-temperature sintering characteristics of tri-rutile $Mg_{0.5}Ti_{0.5}TaO_4$ ceramics. *J. Adv. Ceram.* **2023**, *12*, 296–308. [CrossRef]
23. Cai, J.; Qi, J.; Yang, Y. Colossal permittivity and ultra-low dielectric loss in Nb-doped $SrTiO_3$ ceramics. *J. Adv. Ceram.* **2023**, *12*, 2247–2256. [CrossRef]
24. Liao, Q.W. Investigation on the Structure-Properties Relationship of Ultra-Low Loss $AB(Nb, Ta)_2O_8$ Microwave Dielectric Ceramics. Ph.D. Thesis, Tianjin University, Tianjin, China, 2012.
25. Hu, Z.C.; Yang, H.Y.; Yang, H.C.; Sun, C.L.; Yang, J.; Li, E.Z. Usage of P-V-L bond theory in regulating properties of microwave dielectric ceramics. *J. Inorg. Mater.* **2025**. [CrossRef]
26. Tzou, W.C.; Chen, Y.C.; Yang, C.F.; Cheng, C.M. Microwave dielectric characteristics of $Mg(Ta_{1-x}Nb_x)_2O_6$ ceramics. *Mater. Res. Bull.* **2006**, *41*, 1357–1363.

27. Luo, W.J.; Wang, S.; Zheng, S.Y.; Li, J.N.; Wang, M.L.; Wen, Y.Z.; Li, L.X.; Zhou, J. Dielectric response of ANb_2O_6 (A = Zn, Co, Mn, Ni) columbite niobates: From microwave to terahertz. *J. Adv. Ceram.* **2024**, *13*, 1189–1197.
28. Yang, H. Research on Preparation and Property Modification of New Niobate-Based Microwave Dielectric Ceramics. Ph.D. Thesis, University of Electronic Science and Technology of China, Chengdu, China, 2019.
29. Shi, L. Research on the Microwave Dielectric Performance Regulation and 5G Communication Applications of Tantalate Ceramics. Ph.D. Thesis, University of Electronic Science and Technology of China, Chengdu, China, 2023.
30. Tang, L.; Yang, H.C.; Li, E.Z.; Zhong, C.W. A novel $Na_{1-x}K_xTaO_3$ perovskite microwave dielectric ceramic with high permittivity and high positive temperature coefficient. *J. Adv. Ceram.* **2023**, *12*, 2053–2061.
31. Ali, M.; Iqbal, Y.; Muhammad, R. Phase evolution and microwave dielectric properties of $A_5M_5O_{17}$-type ceramics. *Mater. Sci. Pol.* **2017**, *35*, 362–367.
32. Liu, X.S. Investigation on the Novel Niobate-Tantalate-Based Microwave Dielectric Ceramics with Medium Permittivity. Ph.D. Thesis, Tianjin University, Tianjin, China, 2017.
33. Wu, X.H. Research on Low Loss Medium Niobium/Tantalate Microwave Dielectric Materials and Its Application. Ph.D. Thesis, University of Electronic Science and Technology of China, Chengdu, China, 2024.
34. Fu, Z.F.; Ma, J.L.; Gao, J.; Liu, P. Preparation of $MgNb_2O_6$ powders by using high-energy ball-milling method and the properties of $MgNb_2O_6$ ceramics. *Sci. Technol. Rev.* **2013**, *31*, 62–65.
35. Hu, J.; Lv, X.P.; Zhang, J.; Li, S.; Xv, W.S.; Xv, Q.H. Research progress in the preparation technology of microwave dielectric ceramics. *Inf. Rec. Mater.* **2018**, *19*, 6–8.
36. Liao, L.W.; Zuo, J.; Yang, P.; Liang, J.J.; Peng, Z.J.; Fu, X.L. Synthesis, phase structure and dielectric properties of $CoTiTa_2O_8$ by molten salt method for LTCC application. *J. Mater. Sci. Mater. Electron.* **2024**, *35*, 1179. [CrossRef]
37. Liou, Y.C.; Sung, Y.L. Preparation of columbite $MgNb_2O_6$ and $ZnNb_2O_6$ ceramics by reaction-sintering. *Ceram. Int.* **2008**, *34*, 371–377. [CrossRef]
38. Zhang, L.L.; Yu, H.L.; Song, T.; Shen, T.; Ma, G.H.; Zhang, Y.C.; Wang, H.R.; Tan, K. Research status of low temperature co-firing of microwave dielectric ceramics. *Adv. Ceram.* **2022**, *43*, 246–261.
39. Xue, X.; Li, X.M.; Fu, C.L.; Zhang, Y.; Guo, J.; Wang, H. Sintering characteristics, phase transitions, and microwave dielectric properties of low-firing $[(Na_{0.5}Bi_{0.5})_xBi_{1-x}](W_xV_{1-x})O_4$ solid solution ceramics. *J. Adv. Ceram.* **2023**, *12*, 1178–1188. [CrossRef]
40. Liu, Y.S. Preparation and Characterization of $MgNb_2O_6$-Based Composite Microwave Dielectric Ceramics. Master's Thesis, China University of Geosciences (Beijing), Beijing, China, 2023.

Disclaimer/Publisher's Note: The statements, opinions and data contained in all publications are solely those of the individual author(s) and contributor(s) and not of MDPI and/or the editor(s). MDPI and/or the editor(s) disclaim responsibility for any injury to people or property resulting from any ideas, methods, instructions or products referred to in the content.